Shallow-water acoustic tomography from angle measurements instead of travel-time measurements

Florian Aulanier, Barbara Nicolas, and Jérôme I. Mars
Unité Mixte de Recherche 5216 CNRS, Grenoble Institut National Polytechnique, Université Joseph Fourier, Université Stendhal, 11 Rue des Mathématiques, Grenoble Campus, BP46, F - 38402 Saint Martin d'Hères Cedex, France
Florian.Aulanier@gipsa-lab.grenoble-inp.fr, Barbara.Nicolas@gipsa-lab.grenoble-inp.fr, Jerome.Mars@gipsa-lab.grenoble-inp.fr

Philippe Roux and Romain Brossier
Institut des Sciences de la Terre, Université Joseph Fourier, CNRS Unité Mixte de Recherche 5275, 1381 Rue de la Piscine, Grenoble 38041, France
Philippe.Roux@obs.ujf-grenoble.fr, Romain.Brossier@ujf-grenoble.fr

Abstract: For shallow-water waveguides and mid-frequency broadband acoustic signals, ocean acoustic tomography (OAT) is based on the multi-path aspect of wave propagation. Using arrays in emission and reception and advanced array processing, every acoustic arrival can be isolated and matched to an eigenray that is defined not only by its travel time but also by its launch and reception angles. Classically, OAT uses travel-time variations to retrieve sound-speed perturbations; this assumes very accurate source-to-receiver clock synchronization. This letter uses numerical simulations to demonstrate that launch-and-reception-angle tomography gives similar results to travel-time tomography without the same requirement for high-precision synchronization.

PACS numbers: 43.30.Pc, 43.60.Fg, 43.60.Pt [DD]
Date Received: May 17, 2013 **Date Accepted:** August 19, 2013

1. Introduction

Munk and Wunsch introduced the concept of ocean acoustic tomography (OAT) in 1979, to perform large-scale ocean monitoring (Munk and Wunsch, 1979). Originally travel times were combined with the infinite-frequency ray approximation to invert sound-speed fluctuations from a set of point-to-point acoustic records (Munk and Wunsch, 1979; Howe *et al.*, 1987; Jesus *et al.*, 2006). Combining the information of all of the ray paths, it was then possible to retrieve maps of spatial sound-speed perturbations (Cornuelle, 1985).

However, OAT appeared limited by the interference between multiple arrivals that prevents the identification of each recorded echo with its ray path (Rodriguez and Jesus, 2000). Moreover, for finite frequency signals, ray theory was another physical limitation (Williamson, 1991) that led to the development of diffraction-based approaches (Devaney, 1984; Bowlin, 1991). In particular, the concept of sensitivity kernels (Marquering *et al.*, 1998; Dahlen, 2004) was applied to the context of ocean acoustics by Skarsoulis and Cornuelle (2004). Finally, an unavoidable concern of OAT has always been the practical difficulty associated with the requirement for perfect synchronization between the sets of sources and receivers at long ranges (Spiesberger *et al.*, 1980).

Recent studies have been designed to overcome some of these limitations. In particular, source and receiver arrays on each side of an oceanic waveguide have been used to identify the acoustic arrivals through (double) beamforming (Roux *et al.*, 2008). Indeed array processing allows the separation of wavefronts of different arrivals that would otherwise superimpose (and would thus be useless for tomographic purpose) in the point-to-point approach. As has been demonstrated in different studies (Rodriguez

and Jesus, 2000; Roux *et al.*, 2011), vertical arrays are no longer optional but are an actual requirement in shallow-water tomography. A recent study that dealt with source–receiver arrays at sea showed how to measure and correct for array tilt (Roux *et al.*, 2013). On the other hand, the price paid for perfect synchronization between the source–receiver arrays is clearly higher than with point-to-point recordings. Finally, it was demonstrated recently with tank data that shallow-water tomography performed with this methodology provides good results for local sound-speed, density, and even surface perturbations (Roux *et al.*, 2011; Marandet *et al.*, 2011; Sarkar *et al.*, 2012).

A consequence of the use of source–receiver arrays and double beamforming for tomographic inversion is the extraction of the new observables: The launch and reception angles of every acoustic beam between the arrays. One way to perform OAT would then be to use the variations of these angles instead of those of the travel times.

In a recent paper study, we developed the sensitivity kernel formalism to be used as a forward model with the launch and reception angles as the observables (Aulanier *et al.*, 2013). The present study goes one step further, with the combination of the angle data from a numerical experiment and their corresponding sensitivity kernels, to produce the range and depth inversion of a local sound-speed perturbation. The comparison made with classical travel-time tomography using the same data leads to similar results. In this perspective, angles just appear as an alternative that has the same spatial sampling requirements as travel times for tomography inversion. However, we demonstrate that the main advantage of tomography based on launch and reception angles is that it can be performed without accurate clock synchronization between the two arrays (although synchronization between each of the transducers within each array is still required).

This letter is organized as follows. Section 2 describes the sensitivity kernel approach and the inversion method that is used to infer sound-speed perturbations from the angles and the travel-time measurements. Section 3 shows the inversion results obtained with the angles and the travel-times as the observables of the acoustic tomography. The letter concludes with new opportunities for OAT.

2. Forward problem and inversion method

This study deals with shallow-water waveguides of 1 km to a few kilometers in range, and 10–100 m in depth, and with broadband acoustic signals that have a central frequency in the kilohertz range. In this configuration, the received wavefield has multiply reflected wavefronts after propagation through the waveguide (Roux *et al.*, 2008; Roux *et al.*, 2011). In this context, the use of a waveguide with a source array at one end and a receiver array at the other combined with signal processing makes it possible to: (1) Measure the signal maximum for each acoustic arrival in terms of its travel time (τ) and reception (Θr) and launch (Θe) angles; and (2) associate these observables with the corresponding multi-reflected acoustic beam in the waveguide (Roux *et al.*, 2008; Nicolas *et al.*, 2008).

When the source–receiver arrays are spread over the whole water column, as in Fig. 1(a), the use of aperture-limited subarrays allows the identification of up to 2200 acoustic beams that cover the whole waveguide in range and depth (see Sec. 3 for details). From the time-angle fluctuations measured between a reference (unperturbed) waveguide and a waveguide with a local perturbation δc, the suggested tomography method requires two main steps:

(1) The formulation of the forward problem, which consists of a linear relationship between the sound-speed perturbation (δc) and the time-angle fluctuations ($\delta\tau$, $\delta\Theta r$, $\delta\Theta e$) through the time-angle sensitivity kernels (Aulanier *et al.*, 2013).
(2) The solution of the inverse problem, which is based on a Bayesian approach that uses the measurements of the time and/or angle fluctuations and the time sensitivity kernels and/or the angle sensitivity kernels to retrieve the sound-speed perturbation in the waveguide.

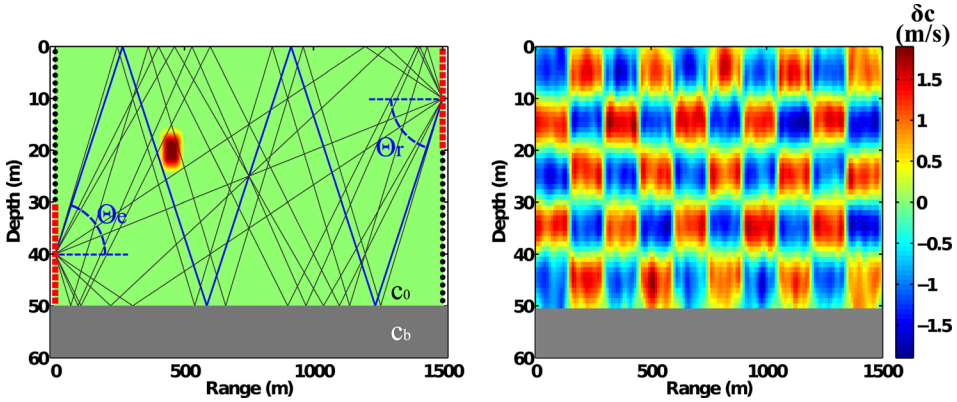

Fig. 1. (Color online) (a) Schematic of the Pekeris waveguide with a set of eigenray paths associated to one pair of source–receiver subarrays (squares) selected among the full vertical arrays (dots). The reception (Θr) and launch (Θr) angles are represented for one multi-reflected path (bold line). The 0.3 m/s sound-speed perturbation is spread over 100 m in range and 10 m in depth. (b) The checkerboard test was performed with the DOA-SK and the DOD-SK. The original checkerboard amplitude was ±1 m/s. The model *a priori* was Gaussian with correlation lengths of 20 m in range and 5 m in depth. The sound speed of the unperturbed waveguide was $c_0 = 1500$ m/s in the water column and $c_b = 1800$ m/s in the bottom.

Focusing on one single beam, the travel-time and angle variations can be measured when a sound-speed perturbation occurs in the waveguide. Considering two states with uniform sound-speed c_0 (unperturbed waveguide) and $c_0 + \delta c$ (waveguide with a small local perturbation), a succession of first-order approximations yields the linear dependence between the sound-speed perturbation (δc) and the observable variations ($\delta\tau$, $\delta\Theta r$, $\delta\Theta e$) through the time-angle sensitivity kernels (Aulanier *et al.*, 2011, Aulanier *et al.*, 2013)

$$\begin{pmatrix} \delta\tau \\ \delta\Theta_r \\ \delta\Theta_e \end{pmatrix} \simeq \iiint_V \begin{pmatrix} K_{TT}(\tau_0, \Theta_{r0}, \Theta_{e0}, r') \\ K_{DOA}(\tau_0, \Theta_{r0}, \Theta_{e0}, r') \\ K_{DOD}(\tau_0, \Theta_{r0}, \Theta_{e0}, r') \end{pmatrix} \delta c(r') dV(r'). \quad (1)$$

In Eq. (1), K_{TT}, K_{DOA} and K_{DOD} are, respectively, the sensitivity kernels of the travel-time (TT-SK), the direction of arrival (DOA-SK), and the direction of departure (DOD-SK) of the acoustic beam that is defined by (τ_0,Θ_{r0},Θ_{e0}), and dV is an elementary volume in the waveguide. A representation of the TT-SK, DOA-SK, and DOD-SK is shown in Fig. 2 for one acoustic beam. Note that these sensitivity kernels

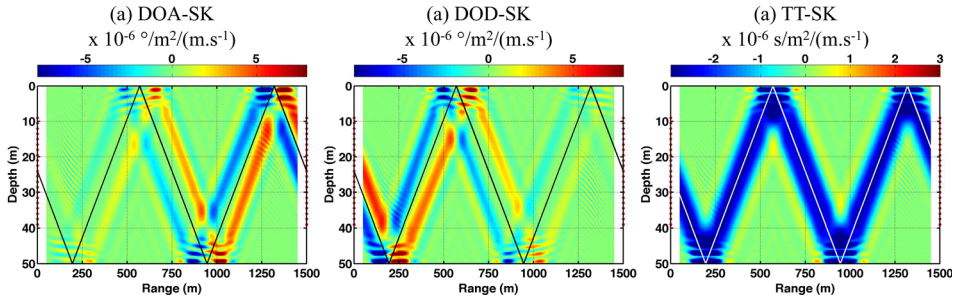

Fig. 2. (Color online) (a) DOA-SK, (b) DOD-SK, and (c) TT-SK associated with one eigenray path with two reflections at the bottom and two reflections at the surface. These sensitivity kernels were computed with a 2-D parabolic equation simulation. The sensitivity kernel amplitudes are relative to a sound-speed change of 1 m/s for a 1-m^2 elementary surface in the waveguide.

were computed from a two-dimensional (2-D) parabolic-equation code (see Sec. 3 for details) for which the elementary volume dV simplifies into an elementary area dS in the waveguide. The sensitivity kernel patterns can be seen as the waveguide sensitivity maps with respect to the travel time and the angle observables associated with one multi-reflected arrival. They clearly differ from one another with each pattern representing the particular observable variations for a local sound-speed perturbation in the waveguide.

In the following, this linearized version of the forward problem is used for acoustic inversion. TT-SK, DOA-SK, and DOD-SK can be used together or independently in the inversion process. The maximum-*a posteriori* (MAP) estimation scheme (Tarantola, 2005; Iturbe *et al.*, 2009; Roux *et al.*, 2011) was implemented to retrieve sound-speed perturbation maps from measurements of travel-time and angle variations. The MAP estimation scheme allows the introduction of *a priori* knowledge of the data misfit and medium parameters. The data misfit *a priori* is taken as being statistically Gaussian and centered. For the sake of simplicity, the data misfit of every beam observables is considered as independent from one another; i.e., the data covariance matrix (C_d) is diagonal. Such an approximation is actually incorrect, although it serves a regularization purpose in the inversion process. The model covariance matrix (C_m) is set in such a way that the sound-speed perturbations are spatially correlated in the medium. According to the diffraction-limited spatial resolution of the source–receiver arrays in the waveguide, the correlation lengths in the range (lr) and depth (lz) can be adjusted with the checkerboard test, which gives the optimal result in the least-mean-square sense [Fig. 1(b)].

Under all these assumptions, the MAP can be expressed as

$$\widehat{m_{MAP}} = m_0 + (G^{-} C_d{}^{-1} G + \lambda C_m{}^{-1})^{-1} G^{-} C_d{}^{-1} (d - G m_0), \tag{2}$$

where $\widehat{m_{MAP}}$ are the voxels of the estimated sound-speed perturbation, G is the sensitivity kernel matrix multiplied by the size of the voxels, d is the vector of the observable variations, and λ is the scalar coefficient introduced to set the weight of the model-versus-data *a priori* during the inversion process, as classically done with the L-curve method (Hansen, 1992; Hansen and O'Leary, 1993). The *a priori* model is $m_0 = 0$, which means that no spatial *a priori* variations are assumed. The last part of this paper deals with the inversion results that compare the angle tomography to travel-time tomography on a numerical dataset.

3. Angle-based acoustic tomography: Numerical validation

A 2-D Padé high-angle parabolic equation code (Collins, 1993) was used to compute the wave propagation in a 1500-m long, 50-m deep Pekeris waveguide without and with a sound-speed perturbation of 0.3 m/s, centered at 450 m in range and 20 m in depth [Fig. 1(a)]. The shape of the perturbation was a 2-D Tukey window of size 100 m (range) × 10 m (depth). The acoustic recordings were performed between two 97-element vertical arrays that covered the whole water column, with an element spacing of 0.5 m. The signal sent by every source to every receiver was a short pulse centered at 2.5 kHz, with a 1.25-kHz bandwidth. From these point-to-point recordings, double beamforming (Roux *et al.*, 2008) was applied on 20-m-aperture source–receiver subarrays (with amplitude shading), to extract a total of 2200 acoustic arrivals that correspond to a large set of multi-reflected acoustic beams with 2–12 reflections on the waveguide interfaces, recorded with 100 pairs of the source–receiver subarray. Eigenrays corresponding to one pair of source–receiver subarrays are shown in Fig. 1(a). For every acoustic arrival, the travel-time and angle variations were measured between the unperturbed and the perturbed waveguide from the parabolic equation computations at a precision of 10^{-6} s in time and 10^{-3} degrees in angle in the absence of noise or surface fluctuations. This corresponds to $<1\%$ of the central period of the signal, and to $<1\%$ of the size of the beam diffraction pattern in this optimal case. The

2200 corresponding TT-SKs, DOA-SKs, and DOD-SKs were also computed on a grid of $76 \times 26 = 1976$ pixels, with a resolution of 20 m in range and 2 m in depth.

The correlation lengths associated with the model *a priori* were set to $lr = 20$ m in range, and $lz = 5$ m in depth. Using *a priori* information obtained from the parabolic equation computations, the data-misfit standard deviation was set to 4.5% of the signal period (0.4 ms) for the travel-time and 2.5% of the main beamforming lobe (3°) for the launch and reception angles. To analyze the spatial resolution of the DOA-SK and DOD-SK models, a checkerboard of ± 1 m/s sound-speed perturbations was generated to induce DOA and DOD variations, which were then inverted using the MAP technique described in the preceding text [Fig. 1(b)]. As expected from the vertical array geometry, the resolution in depth is better than that in range. The resolution is uniform within the waveguide except close to the interfaces.

Figure 3 shows a comparison of the tomography results performed with the angles and with the travel-time data. In both cases, the shape and location of the sound-speed perturbation is correctly imaged. More quantitatively, the sound-speed perturbation is estimated at 0.28 m/s in the case of travel time and 0.29 m/s in the case of angles, for a ground truth of 0.3 m/s. The average background noise level is also very similar, with 7.6e-3 m/s for the travel-time tomography and 5.75e-3 m/s for the angle tomography. Note also the presence of similar artifacts with positive and negative patches around the perturbation.

4. Discussion

In the context of a shallow-water oceanic waveguide, the angle variations of the acoustic beams have been used as observables to invert for the sound-speed perturbations in the same way as the travel time. The angle tomography results are similar to those of the travel-time tomography in terms of the spatial resolution and background noise. At the same time, the use of angles instead of time offers the possibility to avoid the challenge of source–receiver synchronization. Indeed, classical shallow-water tomography requires highly accurate source-to-receiver synchronization that always represents a technical challenge in practice. For example, the optimal synchronization would imply the sharing of the same clock by the sources and receivers, which means that these all need to be wired together. This is impossible, of course, as soon as source–receiver distances exceed a few kilometers. In this case, we are forced to use two independent acquisition systems for the sources and receivers, which are most of the time combined with a multiplexer to switch between the set of sources or receivers on each side. As two clocks can never be exactly the same, this tiny difference results in a small drift between the

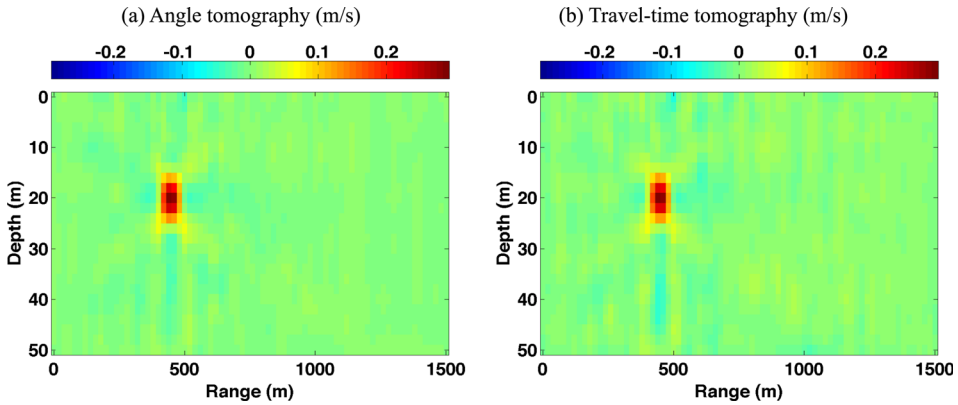

Fig. 3. (Color online) Tomography results obtained with (a) angle variations and (b) travel-time variations. The data consist of 2200 acoustic arrivals [rays with 2–12 reflections at the interfaces (22 rays) recorded by 100 pairs of 20-m-apart source–receiver subarrays]. The model is made up of 1976 pixels.

timing of the two systems. We classically get around this problem by triggering the acquisitions to a GPS clock, for example, on a minute basis. However, even a 10^{-6} relative match of the clocks implies a 15% phase shift that is not negligible at 2.5 kHz after 1 min. Triggering to GPS over less than 1 min is also feasible, but this might then interact with the acoustic acquisition procedure between the set of sources and receivers. Finally, another solution is to record the GPS counts on the two systems and match them in post-processing, but this means the loss of two channels, one for the source and one for the receiver. Instead angle tomography only assumes separate synchronization on each of the source and receiver arrays to beamform the acoustic data with the angles measurement independent of the source-to-receiver synchronicity (Roux, 2013).

Actually, the main inconvenience of the angle-based tomography is the use of highly populated arrays to sample the incident field. However, even travel-time tomography in shallow water requires the separation of the arrival times of the multipath echoes; this requires array processing. In practice, the coverage of the full water column is obviously problematic, although partial coverage is perfectly viable with acoustic tomography goals on a limited set of eigenbeams, which eventually results in a degraded spatial resolution in range/depth. In the present letter, the choice of the full water column coverage was dictated by the objective of the optimal spatial resolution for the tomography inversion (Fig. 3).

Finally, some classical limitations in ocean tomography (bottom roughness and surface dynamic perturbations) might also degrade the quality of the inversion. Further experimental tests on small-scale tank data and under at-sea configurations are needed to confirm the advantages of angle OAT in an operational context to move toward new perspectives in ocean imaging.

Acknowledgments

The authors would like to thank Jit Sarkar for sharing his implementation of the parabolic equation code and Emmanuel Skarsoulis and Bruce D. Cornuelle for helpful comments.

References and links

Aulanier, F., Nicolas, B., Roux, P., and Mars, J. I. (**2011**). "Direction-of-arrival, direction-of-departure and travel-time sensitivity kernels obtained through double beamforming in shallow water," in *UAM Proceedings 2011*, pp. 453–460.

Aulanier, F., Nicolas, B., Roux, P., and Mars, J. I. (**2013**). "Time-angle sensitivity kernels for sound-speed perturbations in a shallow ocean," J. Acoust. Soc. Am. **134**(1), 88–96.

Bowlin, J. (**1991**). "Generating eigenray tubes from two solutions of the wave equation," J. Acoust. Soc. Am. **89**(6), 2663–2669.

Collins, M. D. (**1993**). "A split-step Padé solution for the parabolic equation method," J. Acoust. Soc. Am. **93**, 1736–1742.

Cornuelle, B. D. (**1985**). "Simulations of acoustic tomography array performance with untracked or drifting sources and receivers," J. Geophys. Res. **90**(3), 9079–9088, doi:10.1029/JC090iC05p09079.

Dahlen, F. A. (**2004**). "Resolution limit of traveltime tomography," Geophys. J. Int. **157**(1), 315–331.

Devaney, A. J. (**1984**). "Geophysical diffraction tomography," IEEE Trans. Geosci. Remote Sens. **22**(1), 3–13.

Hansen, P. (**1992**). "Analysis of discrete ill-posed problems by means of the L-curve," SIAM Rev. **34**(4), 561–580.

Hansen, P., and O'Leary, D. (**1993**). "The use of the L-curve in the regularization of discrete ill-posed problems," SIAM J. Sci. Comput. **14**(6), 1487–1503.

Howe, B. M., Worcester, P., and Spindel, R. (**1987**). "Ocean acoustic tomography: Mesoscale velocity," J. Geophys. Res. **92**, 3785–3805, doi:10.1029/JC092iC04p03785.

Iturbe, I., Roux, P., Nicolas, B., Virieux, J., and Mars, J. I. (**2009**). "Shallow-water acoustic tomography performed from a double-beamforming algorithm: Simulation results," IEEE J. Ocean. Eng. **34**(2), 140–149.

Jesus, S. M., Soares, C., Coelho, E., and Picco, P. (**2006**). "An experimental demonstration of blind ocean acoustic tomography," J. Acoust. Soc. Am. **119**(3), 1420–1431.

Marandet, C., Roux, P., Nicolas, B., and Mars, J. I. (**2011**). "Target detection and localization in shallow water: An experimental demonstration of the acoustic barrier problem at the laboratory scale," J. Acoust. Soc. Am. **129**(1), 85–97.

Marquering, H., Nolet, G., and Dahlen, F. A. (**1998**). "Three-dimensional waveform sensitivity kernels," Geophys. J. Int. **132**(3), 521–534.
Munk, W., and Wunsch, C. (**1979**). "Ocean acoustic tomography: A scheme for large scale monitoring," Deep-Sea Res., Part A **26**(2), 123–161.
Nicolas, B., Iturbe, I., Roux, P., and Mars, J. I. (**2008**). "Double formation de voies pour la séparation et l'identification d'ondes: Applications en contexte fortement bruité et à la campagne FAF03" ("Double-beamforming for wave separation and identification: Applications in high-noise level context and on FAF03 at-sea experiment data"), TS. Trait. Signal **25**(4), 293–304.
Rodriguez, O., and Jesus, S. (**2000**). "Physical limitations of travel-time-based shallow water tomography," J. Acoust. Soc. Am. **108**, 6, 2816–2822.
Roux, P. (**2013**). "Acoustical tomography in the shallow water ocean: Dream or reality?" J. Acoust. Soc. Am. **133**, 30407–30416.
Roux, P., Cornuelle, B. D., Kuperman, W. A., and Hodgkiss, W. S. (**2008**). "The structure of raylike arrivals in a shallow-water waveguide," J. Acoust. Soc. Am. **124**(6), 3430–3439.
Roux, P., Iturbe, I., Nicolas, B., Virieux, J., and Mars, J. I. (**2011**). "Travel-time tomography in shallow water: Experimental demonstration at an ultrasonic scale," J. Acoust. Soc. Am. **130**(3), 1232–1241.
Roux, P., Kuperman, W. A., Cornuelle, B. D., Aulanier, F., Hodgkiss, W. S., and Song, H. C. (**2013**). "Analyzing sound speed fluctuations in shallow water from group-velocity versus phase-velocity data representation," J. Acoust. Soc. Am. **133**, 1945–1952.
Sarkar, J., Marandet, C., Roux, P., Walker, S., Cornuelle, B. D., and Kuperman, W. A. (**2012**). "Sensitivity kernel for surface scattering in a waveguide," J. Acoust. Soc. Am. **131**(1), 111–119.
Skarsoulis, E. K., and Cornuelle, B. D. (**2004**). "Travel-time sensitivity kernels in ocean acoustic tomography," J. Acous. Soc. Am. **116**(1), 228–238.
Spiesberger, J., Spindel, R., and Metzger, K. (**1980**). "Stability and identification of ocean acoustic multipaths," J. Acoust. Soc. Am. **67**, 2011–2017.
Tarantola, A. (**2005**). *Inverse Problem Theory and Methods for Model Parameter Estimation* (Elsevier Science, New York), p. 342.
Williamson, P. R. (**1991**). "A guide to the limits of resolution imposed by scattering in ray tomography," Geophysics **56**(2), 202–207.